Progress in Natural Science: Materials International 27 (2017) 416–423

HOSTED BY

Contents lists available at ScienceDirect

Progress in Natural Science: Materials International

journal homepage: www.elsevier.com/locate/pnsmi

Original Research

Sonochemical synthesis of nanostructured nickel hydroxide as an electrode material for improved electrochemical energy storage application

Arshid Numan[a,1], Navaneethan Duraisamy[b,1], Fatin Saiha Omar[a], Dhanaraj Gopi[b], K. Ramesh[a], S. Ramesh[a,*]

[a] Center for Ionics University of Malaya, Department of Physics, Faculty of Science, University of Malaya, Kuala Lumpur 50603, Malaysia
[b] Department of Chemistry, Periyar University, Salem 636011, Tamilnadu, India

ARTICLE INFO

Keywords:
Nickel hydroxide
Sonochemical synthesis
Surface morphology
Electrode materials

ABSTRACT

A facile and fast approach for the synthesis of a nanostructured nickel hydroxide ($Ni(OH)_2$) via sonochemical technique is reported in the present study. The X-ray diffraction results confirmed that the synthesized $Ni(OH)_2$ was oriented in β-phase of hexagonal brucite structure. The nanostructured $Ni(OH)_2$ electrode exhibited the maximum specific capacitance of 1256 F/g at a current density of 200 mA/g in 1 M $KOH_{(aq)}$. $Ni(OH)_2$ electrodes exhibited the pseudocapacitive behavior due to the presence of redox reaction. It also exhibited long-term cyclic stability of 85% after 2000 cycles, suggesting that the nanostructured $Ni(OH)_2$ electrode will play a promising role for high performance supercapacitor application.

1. Introduction

Supercapacitors have attracted great attention as energy storage devices because of their high power density, fast charging time and long lifespan. It can be classified into two types such as electrical double layer capacitor (EDLC) and pesudocapacitor. In EDLC, the electrical charge is stored at the electrode-electrolyte interfaces but in pesudo-capacitor, the charge is stored from reversible faradaic reactions occurred at the electrode-electrolyte interfaces [1–4]. The electrochemical performances of the device are mainly depending on physico-chemical properties of the electro-active materials. Carbon based materials such as activated carbon, graphite, graphene, carbon nanotubes and etc., have been used in EDLC. On the other hand, transition metal oxides/hydroxides and conducting polymers are significantly employed for pesudocapacitor, which are having high energy density than that of EDLC. There are several metal oxides have been used as an electrode materials such as RuO_2, NiO, CuO, MnO_2. TiO_2, MoO_3, etc. The metal oxides have wide band gaps (semiconductors or even insulator nature), which leads to exhibit high specific capacitance but poor electrical conductivity, resulting to limit the power density. Conducting polymers have flexible properties and low-cost. However, they have relatively low specific capacitance (< 100 F/g) and poor cyclic stability due to their chemical instability in the electrolytes [5–7]. These disadvantages can be overcome by introducing alternative inexpensive electrode material of nickel hydroxide ($Ni(OH)_2$) due to low cost, well-defined electrochemical redox nature, and easy to prepare with different structural morphologies.

Nickel hydroxide possess a hexagonal layered morphology with two polymorphs such as α-$Ni(OH)_2$ and β-$Ni(OH)_2$. Upon oxidation, α-$Ni(OH)_2$ is converted into γ-NiOOH at a lower potential than that of oxidation potential range for conversion of β-$Ni(OH)_2$ into β- NiOOH [8,9]. However, it is very hard to synthesis of α-$Ni(OH)_2$ and also unstable during preparation or on storage/testing period in strong alkaline medium, which is quickly transform into β-$Ni(OH)_2$ [10]. Until now, there are different sizes and shapes of nanostructured materials received tremendous attention in electrochemical applications due to the influence of physicochemical properties. For example, Li et al. reported that nanosheet morphology of $Ni(OH)_2$ revealed specific capacitance of 953.67 at 0.2 A/g in presence of 6 M KOH electrolyte [11]. Wang et al. reported fish-like morphology showed the specific capacitance of 1000 F/g at 0.01 A/g [12]. Yang et al. reported that the electrodeposited $Ni(OH)_2$ on Ni foam showed 3D nanostructure with porous morphology with the specific capacitance of 3152 F/g at 4 A/g. The electrochemical performances of $Ni(OH)_2$ are significantly varied with respect to the morphology, which is compared with other energy storage materials as provided in Table 1.

Various methods have been reported to synthesize the nickel hydroxide with different structural morphologies and shapes, such as

Peer review under responsibility of Chinese Materials Research Society.

* Corresponding author.
E-mail addresses: naveennanoenergy@gmail.com (N. Duraisamy), rameshtsubra@gmail.com (S. Ramesh).

[1] Authors are equally contributed.

http://dx.doi.org/10.1016/j.pnsc.2017.06.003
Received 9 December 2016; Received in revised form 30 May 2017; Accepted 2 June 2017
Available online 03 August 2017

Table 1
Summarize the $Ni(OH)_2$ work with latest reported results of energy storage material.

Materials	Synthesis method	Surface morphology	Current Density (A/g)	Specific capacitance (F/g)	Electrolyte	References
$Ni(OH)_2$	Chemical precipitation	Nanosheet	0.2	953.67	6 M KOH	[11]
NiO	Hydrothermal method and followed by calcination	Ball-like structure	0.2	411	2 M KOH	[13]
$Ni(OH)_2$ particles	Repeated immersion method	fish-like shape	0.01	1000	3 M KOH	[12]
NiO	Sonochemical and followed by calcination	Nanocluseter	0.3	448.5	1 M KOH	[14]
$rGO–Co_3O_4$	Hydrothermal	Cubical shape decorated rGO sheet	0.2	278	1 M KOH	[15]
NiO	Electrohydrodynamic atomization	anisotropic nanoplatelets	0.1	110	1 M of KOH	[16]
NiO	surfactant-templated wet chemistry followed by the decomposition	Porous nanosheets	3	993	6 MKOH	[17]
$Ni(OH)_2$	Electrodeposition	3D and porous superstructure	4	3152	3% KOH	[18]
$CdO–Co(OH)_2$	Electrodeposition	Nanoplates	0.01	1119	0.1 M KOH	[19]
Graphene/$Ni(OH)_2$	Mechanically assisted method	Nanoparticles dispersed on graphene sheet (nanocomposite)	4	1568	1 M KOH	[20]
nickel-cobalt layered double hydroxide Nickel-cobalt layered double hydroxide	Hydrothermal	Ultrathin nanosheets	3	2682	1 M KOH	[21]
$NiCo_2O_4$	Hydrothermal	nanoplates	0.375	132	2 M KOH	[22]
$Ni(OH)_2$	Chemical precipitation	Nanosheets	0.3	282.4	6 M KOH	[23]
$Ni(OH)_2$-graphene sheet-carbon nanotube composite	Two step process of Solvo thermaland chemical precipitation	Nanosheets are dispersed into the 3D graphene–CNT framework	0.2	1170.38	6 M KOH	[11]
α-$NiMoO_4$	solution combustion synthesis	Irregular shaped	1.2	1517	2 M NaOH	[24]
$Co(OH)_2$ loaded carbon fiber	Electrodeposition	nanoflakes	0.001	386.5	1 M LiOH	[25]
β-$Ni(OH)_2$ films	Chemical bath deposition	Hierarchical multilayer nanosheets clusters	0.0005 A/cm^2	462	2 M KOH	[26]
Co_3O_4	Electrodeposition	Nanoflakes	6.25	598.9	1 M H2SO4	[27]
$Ni(OH)_2$	Electrodeposition	nanospheres	20	1,868,	1 M KOH	[28]

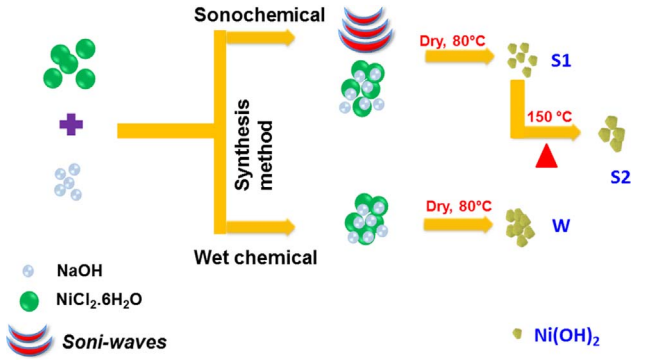

Fig. 1. A schematic representation for the formation of nanostructured $Ni(OH)_2$.

sol-gel, chemical precipitation, electrochemical deposition and chemical bath deposition [8]. Zhu et al. synthesized ultrathin two-dimensional nanosheet of α-$Ni(OH)_2$ via a rapid microwave-assisted liquid-phase growth followed by heat treatment [29]. However, this method needs careful handling because the rapid heating of organic solvents under closed vessel condition may results in explosion. Dubal et al. reported different nanostructured of β-$Ni(OH)_2$ thin films (nanoflakes, nanosheets and honeycomb) prepared via chemical bath deposition using different nickel precursors [26], and this method is simple and only needs solution container and substrate for the sample deposition. Nonetheless, it produces wastage of solution after every sample deposition. Meyer et al. synthesized nanometric platelet-like $Ni(OH)_2$ particles through the polycondensation followed by citrate species coating without the aid of any surfactant or polymer [30]. Even though the method does not require high temperature during the sample synthesis, the procedure was complex to carry out. Qi et al. reported a template method to fabricate β-$Ni(OH)_2$ microspheres with plicate surface [31]. This method is very easy for rapid development of nanomaterials with desired shapes and sizes. However, the elimination of the template may lead to disturb the part of the nanostructures. Liang et al. demonstrated on low-cost production of β-Ni-$(OH)_2$ nanosheets synthesized using hydrothermal method [32]. However, the method relies upon high temperature along with extended processing durations. Apart from these, there is another method to synthesis nanostructured materials without using any surfactant and complex process, i.e., called as sonochemical method. The basic principles of sonochemistry mainly depend on the acoustic cavitation phenomenon such as the nucleation, growth and smaller size bubbles collapse aggressively in presence of liquid medium. Furthermore, rapidly high temperature (> 5000 °C), excess pressure (> 500 atm) and very high cooling rate (10^{10} K/s) arises throughout the sonication process, which are significantly influence on structural morphology, sizes of synthesizing materials [14,33].

Here, we report the synthesis of nanostructured nickel hydroxide by facile and fast growing technique of sonochemical method and followed by calcination process. The non-aggregated nickel hydroxide is playing a major role in the selection of electrode material for energy storage application, which is clearly investigated via structural crystallinity, surface morphology and electrochemical measurements.

2. Materials and methods

2.1. Materials

Nickel chloride hexahydrate ($NiCl_2{\cdot}6H_2O$), sodium hydroxide (NaOH) were received from Sigma-Aldrich. All chemicals used throughout the experiments were of analytical grade. The sonication process (fisher scientific, model 120 sonic dismembrator, titanium horn used as a sonication probe) was used to synthesis nanostructured nickel hydroxides.

2.2. Synthesis of nanostructured nickel hydroxide

For the preparation of nanostructured nickel hydroxide, 1 M of $NiCl_2{\cdot}6H_2O$ was completely dissolved in 50 ml of deionized water under constant stirring for 10 min. As-prepared NaOH (2 M) was added drop wise into the above solution under sonication process using an ultrasonic probe. This reaction was continuing for 1 h without any coolant, leading to attain the reaction temperature about 60 ± 5 °C [14]. This temperature was further enhancing the chemical reaction during sonication process. The entire sonication process was carried out with 75% of amplitude. The obtained product was washed several times with deionized water and collected through centrifugation. Finally, the synthesized sample was dried at 80 °C for 24 h in an electric furnace. Similarly, the experiment was repeated under same condition with calcination at 150 °C for 3 h. Additionally, the controlled experiment was carried out using wet-chemical method for comparison with sonochemically synthesized materials. The detailed wet-chemical process was given in supporting document (Section 1). Therefore, the synthesized nickel hydroxide samples are represented as S1 (*as*-prepared by sonication), S2 (sonicated and followed by calcination at 150 °C) and W (as-prepared by wet-chemical method). The schematic representation of the whole experiments is represented in Fig. 1.

2.3. Fabrication of working electrodes

The electrochemical properties of synthesized materials were examined by cyclic voltammetry (CV), electrochemical impedance (EIS) and galvanostatic charge-discharge (GDC) using electrochemical workstation (Gamry, Interface1000 (Warminster, PA, USA). The electrochemical behaviors were examined in three electrode cell. Herein, nickel hydroxide coated Ni-foam, Ag/AgCl and platinum (Pt) are denoted as a working, reference and counter electrodes respectively. The entire experiment was executed in 1 M KOH as an aqueous electrolyte at room atmospheric condition. The working electrode was prepared via mixing 75 wt% of $Ni(OH)_2$ (S1) with 15 wt% of acetylene black and 10 wt% polyvinylidene difluoride (PVdF) in 1-methyl-2-pyrrolidinone (NMP) as the solvent under sonication to attain a homogeneous slurry. An aliquot (5 μL) of slurry was used to coat on cleaned nickel (Ni) foam (coating area: 1×1 cm^2). This process was repeated to fabricate other two electrodes using synthesized materials of S2 and W. The mass loading of active material on nickel foam was ~ 4.6 mg.

2.4. Characterization techniques

The structural crystallinity was examined through X-ray diffractometer (Philips, X′ pert) using a Cu Kα radiation source of wavelength λ = 1.5406 Å, which was measured in the range of 2θ = 20–70° with a step of 0.02°. The Fourier transform infrared spectrum was recorded with Thermo Scientific Nicolet iS10 spectrophotometer. The surface morphology of nanostructured nickel hydroxide samples were investigated by field emission scanning electron microscopy (FE-SEM) (JSM-7600F; operated at 5–20 kV).

3. Results and discussion

3.1. Structural analysis

The structural crystallinity of synthesized nickel hydroxides were examined by XRD analysis. Fig. 2a illustrates the XRD patterns of W, S1 and S2. All the diffraction peaks of (001), (100), (101), (102) and (110) are well indexed as a hexagonal structure of β-$Ni(OH)_2$ (JCPDS 14–0117) with a space group of *p-3m1(164)*. The hexagonal structure of β-$Ni(OH)_2$ illustrated lamellar structure, where NiO_6 octahedra were detached through hydrogen atoms [34]. The lowest grain size was

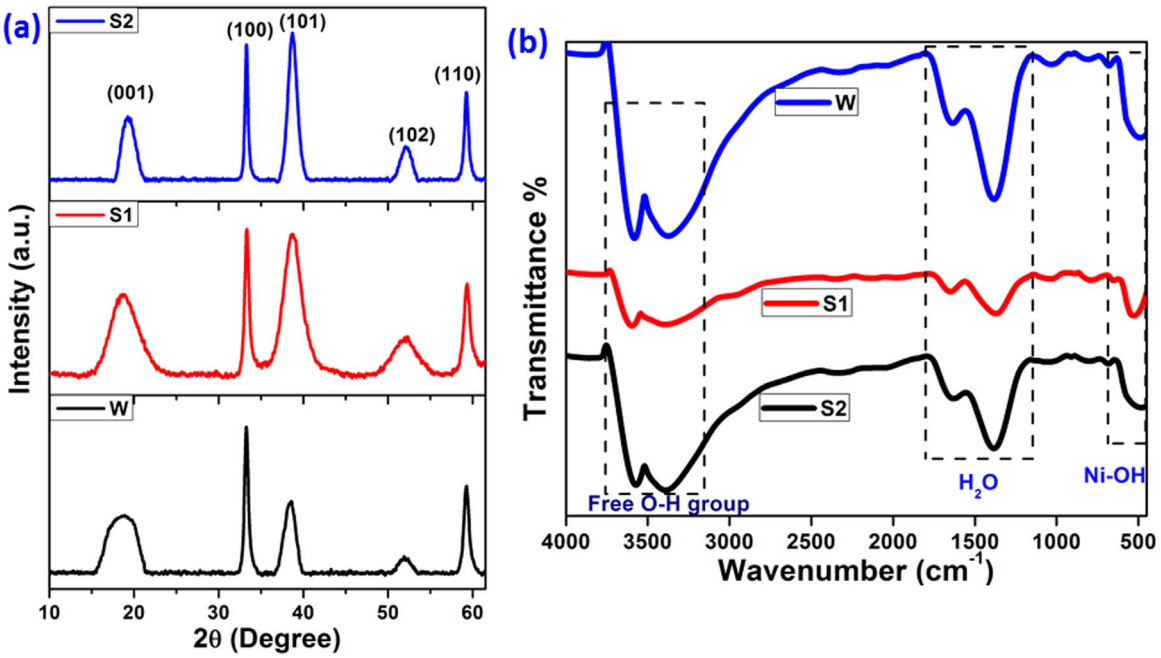

Fig. 2. (a) X-ray diffraction pattern of $Ni(OH)_2$ samples (S1, S2 and W) and (b) FT-IR analysis of nanostructured $Ni(OH)_2$ samples.

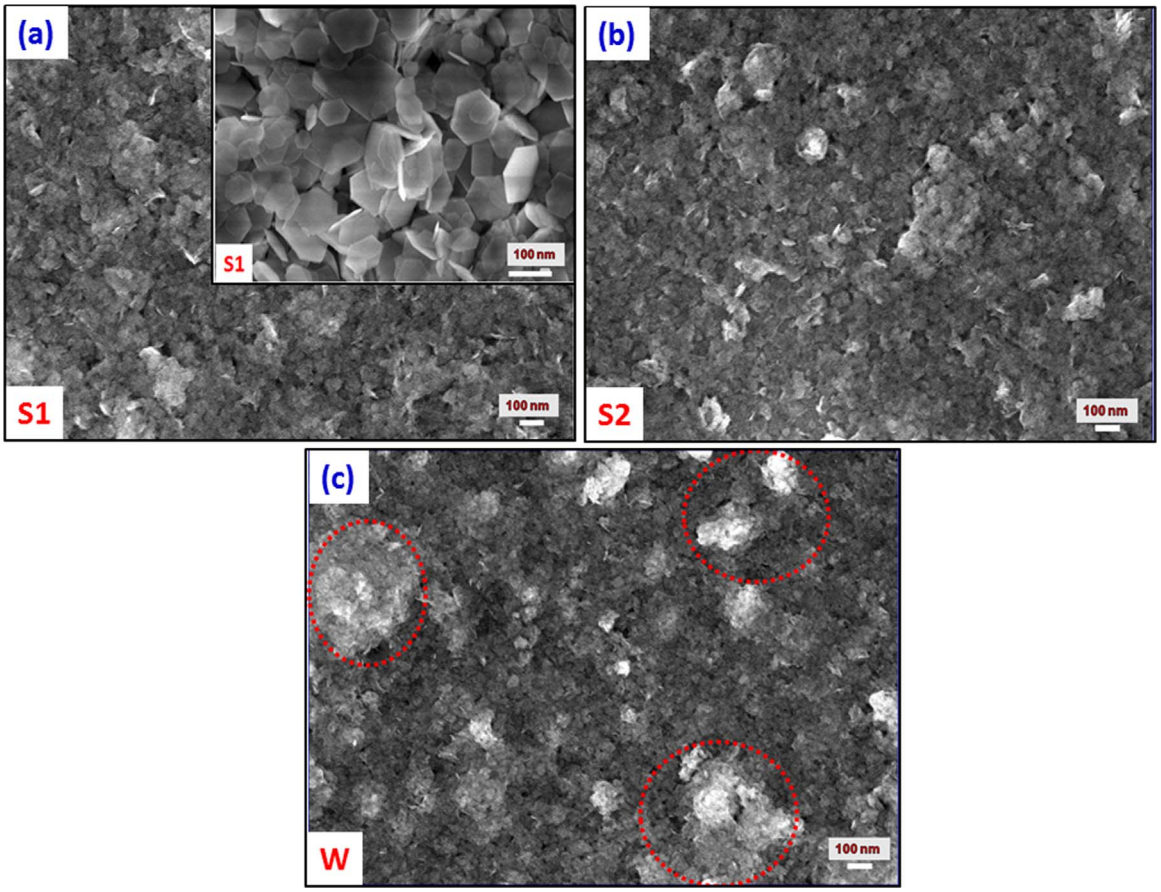

Fig. 3. FESEM images: (a) S1, (b) S2, (c) W and inset in (a) shows the high magnification image of sample S1.

observed in S1 sample, which is confirmed by peak broadening in XRD pattern (Fig. 2a). No other characteristic peaks were observed, suggesting the purity of β-$Ni(OH)_2$ samples.

The FT-IR spectra of synthesized nanostructured $Ni(OH)_2$ samples are shown in Fig. 2b. The O–H stretching mode is absorbed at 3610 and 3412 cm^{-1}, which is due to the presence of free O–H group in β-$Ni(OH)_2$ structure [26]. The absorption peak at 531 cm^{-1} corresponds to Ni–OH stretching vibration for $Ni(OH)_2$ sample [26]. The absorption of broad band at 1640–1400 cm^{-1} corresponds to bending vibration of water molecules, which may occur from atmospheric moisture. Further, the presence of hydroxyl group confirmed the formation of $Ni(OH)_2$. The FT-IR study is in good agreement with the XRD results.

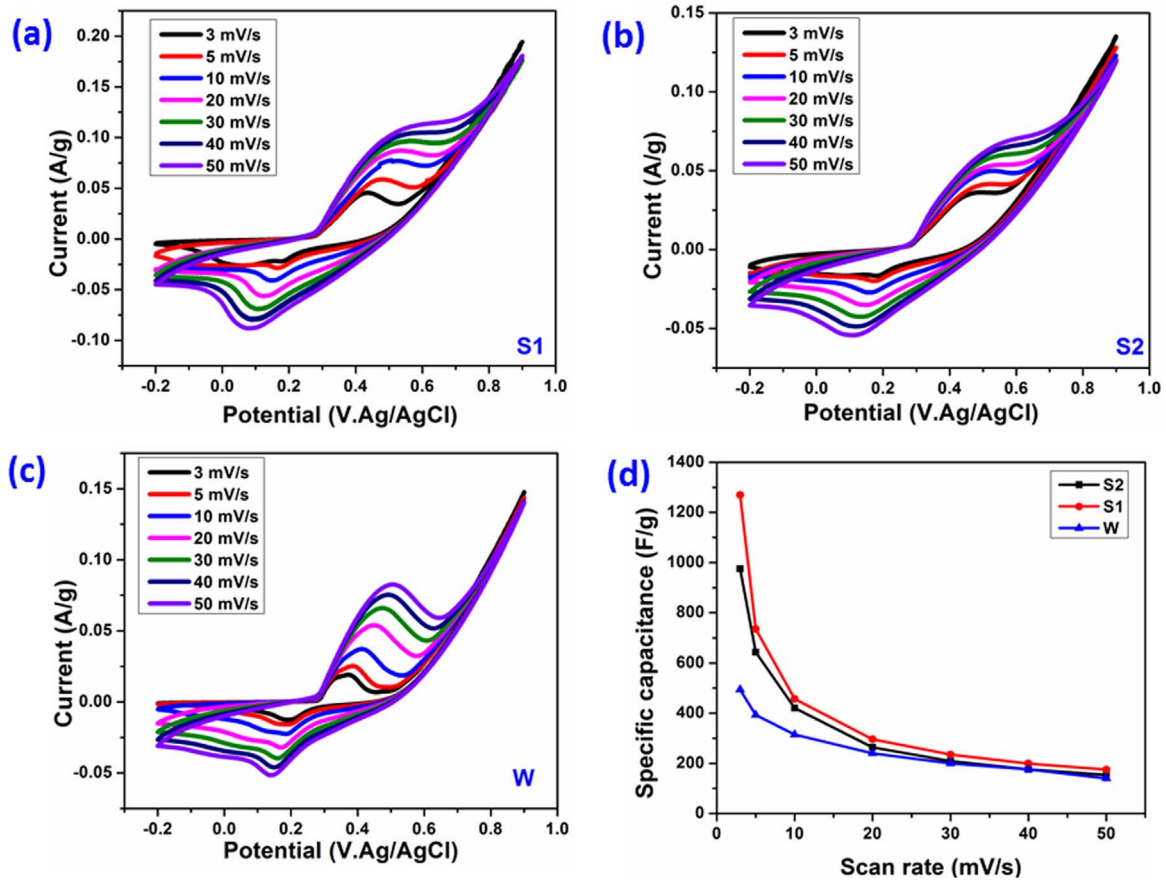

Fig. 4. CV curves obtained for the different nanostructured $Ni(OH)_2$ electrodes at different scan rates (a) S1, (b) S2 and (c) W, (d) specific capacitance of $Ni(OH)_2$ electrodes at different scan rates.

The surface morphologies of synthesized samples were clearly examined by FE-SEM analysis. Fig. 3 shows the surface morphology of $Ni(OH)_2$ samples (S1, S2 and W). Fig. 3a illustrates the uniform distribution of nanostructured $Ni(OH)_2$ (S1) with free of particle aggregation, which is due to the effect of sonication lead to avoid the nanosized particle aggregation. Inset in Fig. 3a (high magnification image) shows the hexagonal shaped $Ni(OH)_2$ (S1) thin flaks with fewer aggregations. However, Fig. 3c reveals the large particle aggregation (indicated by the circle) in sample W because of non-sonication, suggesting poor electrochemical performance. S2 sample may also demonstrate a few aggregations due to the effect of calcination process (leading to coagulate the smaller particles with rougher surface) (Fig. 3b). Therefore, the surface morphology confirms that the sample S1 will have superior electrochemical performance than that of S2 and W.

3.2. Electrochemical performance

The capacitive performance of synthesized $Ni(OH)_2$ electrodes were examined via various electrochemical studies, including CV, EIS and galvanostatic charge-discharge techniques. Fig. 4(a-c) shows the CV curves of S1, S2 and W electrodes at different scan rates in 1 M KOH electrolytes. It was observed that all CV curves revealed one pair of redox peaks, suggesting the pseudocapactive behavior of $Ni(OH)_2$ electrodes. Here, the anodic peak was observed due to the oxidation of $Ni(OH)_2$ into NiOOH and the cathodic peak was attained for the reverse process. The well-defined surface faradic reaction will proceed according to the following reaction [28].

$$Ni(OH)_2 + OH^- \leftrightarrow NiOOH + H_2O + e^- \quad (1)$$

The S1 electrode revealed a higher integrated area than that of other two electrodes (S2 and W), which is further confirmed the excellent electrochemical performance of S1 sample. The specific capacitances (C_{sp}) of electrodes are calculated by the following equation [15].

$$Cs = \frac{\int IdV}{v \times m \times \Delta V} \quad (2)$$

Where, C_s is the specific capacitance of prepared electrode (F/g), v is the scan rate (V/s), m is the mass of active material ($Ni(OH)_2$) (g), ΔV is the applied potential window, and the integral term is equal to the area under the CV curve. Herein, the calculated C_{sp} of electrodes at a scan rate of 3 mV/s represented as 1256, 975 and 494 F/g corresponds to S1, S2 and W respectively. The maximum specific capacitance was observed in S1 due to the sonication lead to attain smaller particle size with non-aggregated morphology, resulting to enhance the electrochemical performance. Moreover, S2 sample also give comparatively good specific capacitance but less than S1 due to the larger particle size with fewer aggregation. In the case of W, the sample revealed the low specific capacitance because of particle aggregations (Fig. 3c), which lead to limit the ions movements in electrode/electrolyte interfaces [35]. Fig. 4d represented that the C_{sp} decreased with increasing scan rates in all electrodes. At low scan rate, the hydroxyl (OH^-) ions had enough time to diffuse into the working electrode. But at high scan rate, the diffusion of ions had less time to intercalate into the respective electrode, suggesting the higher specific capacitance values at lower scan rate than that of high scan rate. Moreover, the anodic and cathodic peaks shifted towards the positive and negative regions, which are good agreement with the previous work reported in literatures [28]. The maximum C_{sp} of 1270 F/g was observed for S1 due to good charge movements and large specific surface area [28]. Further investigation on galvanostatic charge-discharge analysis for $Ni(OH)_2$ electrodes was

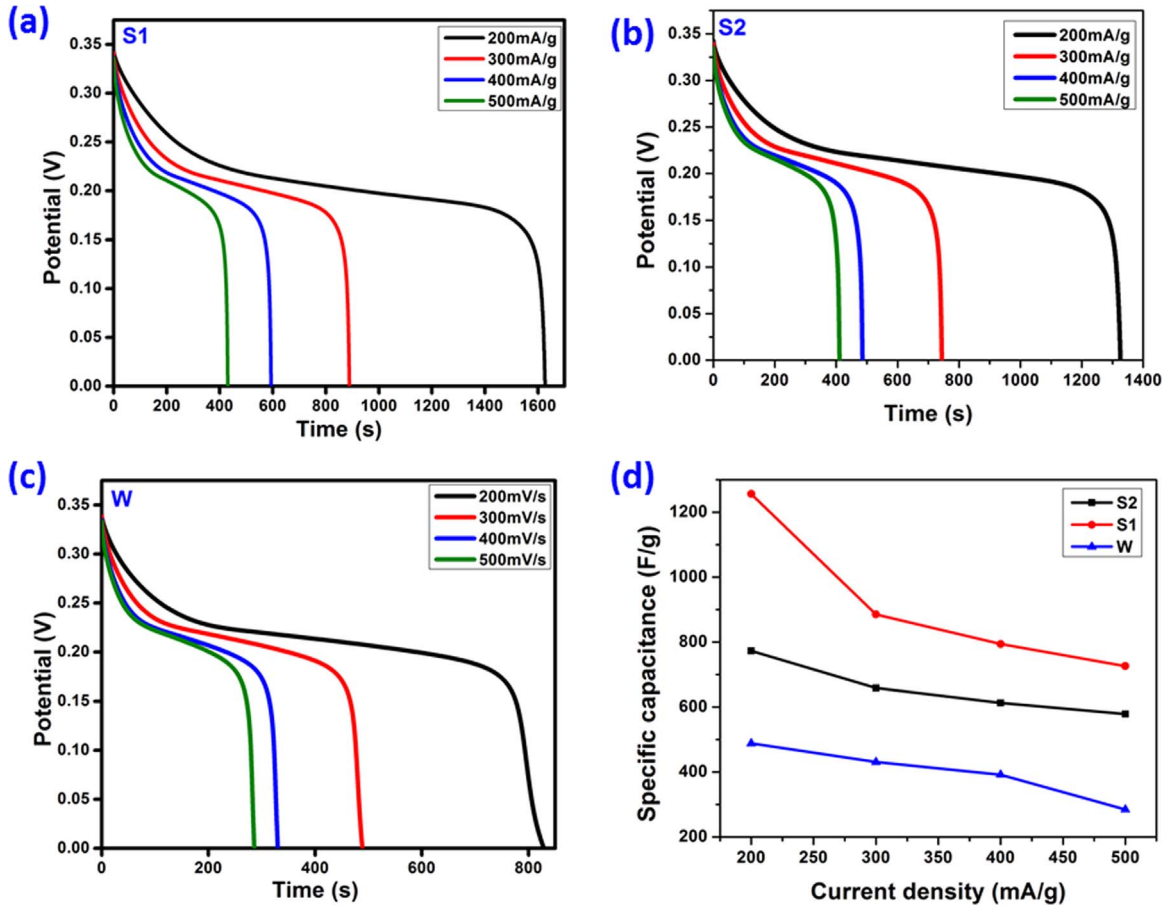

Fig. 5. The galvanostatic discharge curves of nanostructured $Ni(OH)_2$ electrodes at different current density, (a) S1, (b) S2 and (c) W, (d) specific capacitance with respect to current densities.

Table 2
Performance comparison of $Ni(OH)_2$ with previously reported works.

Materials	Synthesis method	Specific capacitance (F/g)	Current Density (A/g)	Cycles number	Cyclic retention (%)	References
$Ni(OH)_2$	Chemical precipitation	953.67	0.2	1000	74.52	[11]
$Ni(OH)_2$-graphene sheet-carbon nanotube composite	Two step process of Solvo thermaland chemical precipitation	1170.38	0.2	1000	89.65	[11]
$Ni(OH)_2$ particles	Repeated immersion method	1000	0.01	200	95	[12]
β-$Ni(OH)_2$ films	Chemical bath deposition	462	0.0005 A/cm^2	1000	89	[26]
$Ni(OH)_2$	Mechanically assisted method	784	4	1000	62	[36]
Graphene/$Ni(OH)_2$ nanocomposites	Mechanically assisted method	1568	4	1000	75	[36]
$Ni(OH)_2$	Chemical precipitation	282.4	0.3	–	–	[23]
$Ni(OH)_2$	Electrodeposition	3152	4	300	52	[37]
$Ni(OH)_2$	**Sonochemical**	**1256**	**0.2**	**2000**	**85**	**This work**

carried out to evaluate the specific capacitance and electrode stability. The galvanostatic discharges curve of electrodes are demonstrated in presence of 1 M KOH electrolyte at different current densities (200 ~ 500 mA/g). All electrodes revealed that the discharge time decreased with increasing the current density, as shown in Fig. 5(a-c). The semi-symmetric discharge curves confirmed the typical pseudocapacitive behavior of $Ni(OH)_2$ electrodes, which is due to the redox reaction at the electrode/electrolyte interface [26]. These results are in good agreement with the CV curves. Moreover, S1 exhibited the longer discharge time than that of other samples due to closely packed arrangements of smaller particles with less particles aggregation.

The specific capacitance of $Ni(OH)_2$ electrodes were calculated from the galvanostatic discharge curves using the following equation [6].

$$Cs = \frac{I \times \Delta t}{\Delta V \times m} \quad (3)$$

where, C_s is the specific capacitance of the active electrode (F/g), I is the current (A), m is the mass of the NiO as the active material (g), ΔV is the potential window, and Δt is the discharge time (s). The obtained specific capacitance values of S1, S2 and W corresponds to 1256, 772.5 and 488.4 F/g at current density of 200 mA/g. The maximum specific capacitance of 1256 F/g was observed in S1 electrode due to the efficient charge transport between the electrolyte and electrode surface. The specific capacitance values decreases with increase in current densities as shown in Fig. 5d. This is due to the following reasons; (i) at low current density, the OH^- ions have adequate time to penetrate into the surface of $Ni(OH)_2$ electrode. However, at high current density, the ions have less time to penetrate, which lead to reduce the specific

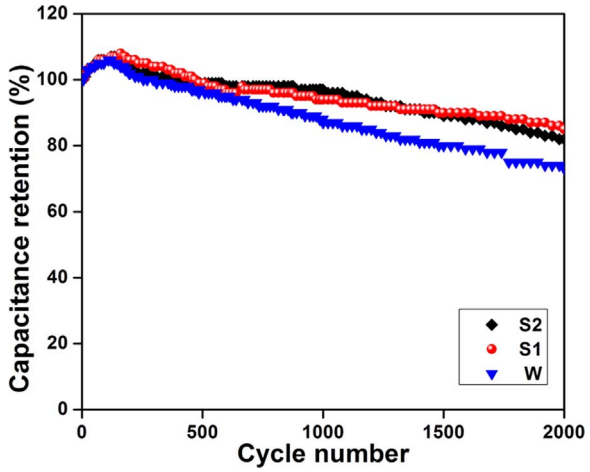

Fig. 6. Capacitance retention with respect to cycle number of nanostructured $Ni(OH)_2$ electrodes (S1, S2 and W).

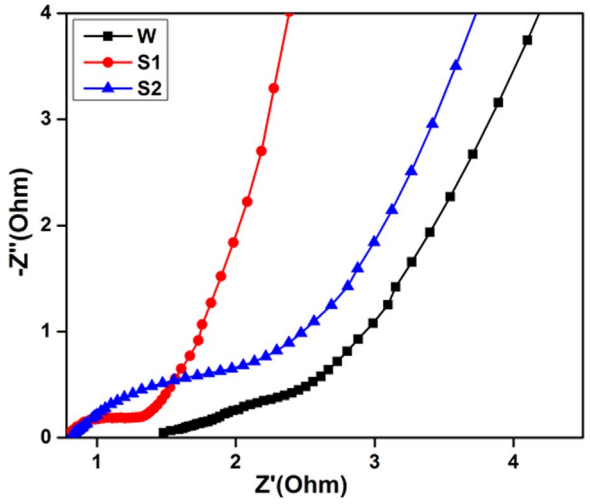

Fig. 7. Nyquist plot of $Ni(OH)_2$ electrodes.

capacitance, (ii) while increasing the current density, the large voltage (IR) drop is observed, which also lead to decrease the specific capacitance (as shown in Fig. S1) [26]. The performance comparison of $Ni(OH)_2$ with previously reported works in literatures are given in Table 2. Fig. S2 illustrates the interactions of OH^- ions on the electrode surface during charging and discharging process. The electrochemical utilization of the active electrode is calculated from the Eq. (4).

$$z = C\Delta V\frac{M}{F} \tag{4}$$

Where, C is the value of specific capacitance (F/g) at 200 mA/g, ΔV is the potential window, M is the molecular weight of nickel hydroxide (92.708 g), and *F* is the faradaic constant. Here, z value is equal to one mean that the entire electroactive materials contributed in the redox process. But, in this work, the calculated *z* values are found to be 0.415, 0.254 and 0.159 correspond to S1, S2 and W, respectively. These values confirmed that 41.5% of active sites are involved for redox process in $Ni(OH)_2$ at S1 sample. This is comparatively higher than that of S2 (25.4%), W (15.9%) samples and nanostructured NiO (14–15%) as reported in the literatures [36,38]. The cyclic stability test of $Ni(OH)_2$ electrodes is an important parameter for their practical application. The cycle stability of nanostructured $Ni(OH)_2$ electrodes were employed in charge-discharge analysis at current density of 6 A/g for 2000 cycles. Fig. 6 illustrates the capacitance retention vs. number of cycles. Initially, the cyclic stability increased up to 200 cycles due to gradual activation of $Ni(OH)_2$ and also enhanced the penetration of the electrolyte ions into the active material [23,39]. Whereas, electrode stability slightly decreased after 200 cycles and remains stable for 2000 cycles. The larger cyclic stabilities were achieved in S1 and S2 samples than W due to the influence of sonication process [14]. Moreover, S1 exhibited optimal cyclic stability (85%) with maximum specific capacitance (1256 F/g) than that of other two samples, which may be due to smaller particles sizes with fewer aggregations, suggesting effective ion transfer from electrolytes to the electrode surface.

EIS measurement was used to investigate the fundamental performance of the active electrode materials for energy application. EIS measurement was conducted in the frequency range of 0.01−100 kHz using an open circuit potential. Generally, the frequency range is divided into two parts, such as, high-frequency and low frequency regions correspond to the semicircle arc and vertical line respectively. The transition between the two regions is named as knee frequency. Typical Nyquist plots of the S1, S2 and W electrodes are represented in Fig. 7. The semicircular arc at high frequency range corresponds to the charge transfer resistance (R_{ct}) at the contact interface between electrolyte and electrode. The straight line slop in the low frequency region denotes the diffusion resistance (Warburg impedance, *W*) of the electrolyte ions into the pore structure of electrode surface. The vertical line in the low-frequency range represents rapid ion diffusion in the electrolyte solution and adsorption onto the electrode surface [37,40]. The lower R_{ct} value (1.30 Ω) was observed in S1 electrode, resulting in improving the charge transfer performance of S1 than the other electrodes. This is due to the smaller particle size with effective electroactive surface area (good electrochemical utilization) of the electrode [14]. Therefore, the above results confirmed that the nanostructured $Ni(OH)_2$ with smaller particle size will play a significant role in supercapacitor application.

4. Conclusion

The nanostructured $Ni(OH)_2$ has been synthesized using sonochemical method, and there structural crystallinity and surface purity clearly investigated via XRD and FT-IR analysis. The uniform distribution of nanostructured $Ni(OH)_2$ with non-aggregated morphology is achieved by ultrasonic waves. The sonicated $Ni(OH)_2$ (S1) exhibites maximum specific capacitance of 1256 F/g at a current density of 200 mA/g with longer cyclic stability (85% for 2000 cycles) than that of other samples (S2 and W). The impedance measurement discloses the low charge-transfer resistance of 1.30 Ω in S1 sample. Therefore, these results confirm that the non-aggregated surface morphology of $Ni(OH)_2$ plays a vital role in electrochemical performance for energy storage application.

Acknowledgements

This work was supported by the High Impact Research Grant (H-21001-F000046) from Ministry of Education, Malaysia, Post-graduate Research Grant (PG034-2015A) and University of Malaya Research Grant (RP025A-14AFR) from University of Malaya. One of the author Dr. Navaneethan Duraisamy acknowledges UGC-Dr. D.S. Kothari Postdoctoral Fellowship (Ref no: No.F.4-2/2006 (BSR)/EN/15–16/0031).

Appendix A. Supporting information

Supplementary data associated with this article can be found in the online version at doi:10.1016/j.pnsc.2017.06.003.

References

[1] W. Yang, Z. Gao, J. Wang, B. Wang, Q. Liu, Z. Li, T. Mann, P. Yang, M. Zhang, L. Liu, Electrochim. Acta 69 (2012) 112–119.
[2] Q. Qu, S. Yang, X. Feng, Adv. Mater. 23 (2011) 5574–5580.

[3] M.Y. Chong, A. Numan, C.W. Liew, K. Ramesh, S. Ramesh, J. Appl. Polym. Sci. 134 (1–11) (2017) 44636.
[4] S. Murali, D.R. Dreyer, P. Valle-Vigon, M.D. Stoller, Y. Zhu, C. Morales, A.B. Fuertes, C.W. Bielawski, R.S. Ruoff, Phys. Chem. Chem. Phys. 13 (2011) 2652–2655.
[5] K. Xie, J. Li, Y. Lai, W. Lu, Z. Zhang, Y. Liu, L. Zhou, H. Huang, Electrochem. Commun. 13 (2011) 657–660.
[6] F.S. Omar, A. Numan, N. Duraisamy, S. Bashir, K. Ramesh, S. Ramesh, RSC Adv. 6 (2016) 76298–76306.
[7] A. Pramanik, S. Maiti, S. Mahanty, Dalton. Trans. 44 (2015) 14604–14612.
[8] S. Xing, Q. Wang, Z. Ma, Y. Wu, Y. Gao, Mater. Lett. 78 (2012) 99–101.
[9] P. Jeevanandam, Y. Koltypin, A. Gedanken, Nano. Lett. 1 (2001) 263–266.
[10] B. Mavis, M. Akine, J. Power Sources 134 (2004) 308–317.
[11] Y. Liu, G. Yuan, Z. Jiang, Z. Yao, M. Yue, J. Alloy. Compd. 618 (2015) 37–43.
[12] K. Wang, L. Li, T. Zhang, Int. J. Electrochem. Sci. 8 (2013) 6252–6257.
[13] P. Justin, S.K. Meher, G. Ranga Rao, J. Phys. Chem. C 114 (2010) 5203–5210.
[14] N. Duraisamy, A. Numan, F.S. Omar, K. Ramesh, S. Ramesh, J. Colloid Interface Sci. 471 (2016) 136–144.
[15] A. Numan, N. Duraisamy, F.S. Omar, Y.K. Mahipal, K. Ramesh, S. Ramesh, RSC Adv. 6 (2016) 34894–34902.
[16] N. Duraisamy, A. Numan, K. Ramesh, K.H. Choi, S. Ramesh, S. Ramesh, Mater. Lett. 161 (2015) 694–697.
[17] X. Sun, G. Wang, J.-Y. Hwang, J. Lian, J. Mater. Chem. 21 (2011) 16581–16588.
[18] G.W. Yang, C.L. Xu, H.L. Li, Chem. Commun. (2008) 6537–6539.
[19] K.K. Tehare, M.K. Zate, S.T. Navale, S.S. Bhande, S.L. Gaikwad, S.A. Patil, S.K. Gore, M. Naushad, S.M. Alfadul, R.S. Mane, Arab. J. Chem. (2017). http://dx.doi.org/10.1016/j.arabjc.2016.01.006.
[20] Z. Sun, X. Lu, Ind. Eng. Chem. Res. 51 (2012) 9973–9979.
[21] H. Chen, L. Hu, M. Chen, Y. Yan, L. W, Adv. Funct. Mater. 24 (2014) 934–942.
[22] T. Kim, A. Ramadoss, B. Saravanakumar, G.K. Veerasubramani, S.J. Kim, Appl. Surf. Sci. 370 (2016) 452–458.
[23] Q. Li, H. Ni, Y. Cai, X. Cai, Y. Liu, G. Chen, L.Z. Fan, Y. Wang, Mater. Res. Bull. 48 (2013) 3518–3526.
[24] B. Senthilkumar, K.V. Sankar, R. Kalai Selvan, M. Danielle, M. Manickam, RSC Adv. 3 (2013) 352–357.
[25] A.D. Jagadale, G. Guana, X. Dua, X. Hao, X. Li, A. Abudula, RSC Adv. 5 (2015) 56942–56948.
[26] D.P. Dubal, V.J. Fulari, C.D. Lokhande, Microporous Mesoporous Mater. 151 (2012) 511–516.
[27] F.S.H. Kazemia, A. Asghari, M.A. kian, Electrochim. Acta 138 (2014) 9–14.
[28] H.B. Li, M.H. Yu, F.X. Wang, P. Liu, Y. Liang, J. Xiao, C.X. Wang, Y.X. Tong, G.W. Yang, Nat. Commun. 4 (1–7) (2013) 1894.
[29] Y. Zhu, C. Cao, S. Tao, W. Chu, Z. Wu, Y. Li, Sci. Rep. 4 (2014) 1–7.
[30] M. Meyer, A. Bee, D. Talbot, V. Cabuil, J.-M. Boyer, B. Repetti, R. Garrigos, J. Colloid Interface Sci. 277 (2004) 309–315.
[31] G. Qi, Y. Liu, W. Jiao, L. Zhang, Micro Nano. Lett. 5 (2010) 278–281.
[32] Z.-H. Liang, Y.-J. Zhu, X.-L. Hu, J. Phys. Chem. B 108 (2004) 3488–3491.
[33] F.S. Ertaş, F.E. Saraç, U. Ünal, Ö. Birer, J. Solid. State Electrochem. 19 (2015) 3067–3077.
[34] R. Wang, J. Lang, Y. Liu, Z. Lin, X. Yan, NPG Asia Mater. 7 (2015) 1–7.
[35] W. Jiao, L. Zhang, Curr. Appl. Phys. 16 (2016) 115–119.
[36] Z. Sun, X. Lu, Ind. Eng. Chem. Res. 51 (2012) 9973–9979.
[37] G.W. Yang, C.L. Xu, H.L. Li, Chem. Commun. (2008) 6537–6539.
[38] S. Vijayakumar, S. Nagamuthu, G. Muralidharan, ACS Appl. Mater. Interfaces 5 (2013) 2188–2196.
[39] J. Ji, L.L. Zhang, H. Ji, Y. Li, X. Zhao, X. Bai, X. Fan, F. Zhang, R.S. Ruoff, ACS Nano. 7 (2013) 6237–6243.
[40] R. Ananthakumar, J.K. Sang, Carbon 63 (2013) 434–445.